MNRAS **000**, 1–12 (2016) Preprint 19 October 2016 Compiled using MNRAS LATEX style file v3.0

On the East-West Longitudinally Asymmetric Distribution of Solar Proton Events

H.-Q. He[1⋆] and W. Wan [1]
[1] *Key Laboratory of Earth and Planetary Physics, Institute of Geology and Geophysics, Chinese Academy of Sciences, Beijing 100029, China*

19 October 2016

arXiv:1610.05489v1 [physics.space-ph] 18 Oct 2016

ABSTRACT
A large data set of 78 solar proton events observed near the Earth's orbit during 1996-2011 is investigated. An East-West longitudinal (azimuthal) asymmetry is found to exist in the distribution of flare sources of solar proton events. With the same longitudinal separation between the flare sources and the magnetic field line footpoint of observer, the number of the solar proton events originating from solar sources located on the eastern side of the nominal magnetic footpoint of observer is larger than the number of the solar proton events from solar sources located on the western side. We emphasize the importance of this statistical investigation in two aspects. On the one hand, this statistical finding confirms our previous simulation results obtained by numerically solving five-dimensional Fokker-Planck equation of solar energetic particle (SEP) transport. On the other hand, the East-West longitudinally (azimuthally) asymmetric distribution of solar proton events accumulated over a long time period provides an observational evidence for the effects of perpendicular diffusion on the SEP propagation in the heliosphere. We further point out that, in the sense of perpendicular diffusion, our numerical simulations and statistical results of SEP events confirm each other. We discuss in detail the important effects of perpendicular diffusion on the formation of the East-West azimuthal (longitudinal) asymmetry of SEP distribution in two physical scenarios, i.e., "multiple SEP events with one spacecraft" and "one SEP event with multiple spacecraft". A functional relation $I_{max}(r) = kr^{-1.7}$ quantifying the radial dependence of SEP peak intensities is obtained and utilized in the analysis of physical mechanism. The relationship between our results and those of Dresing et al. is also discussed.

Key words: diffusion – turbulence – cosmic rays – Sun: particle emission

1 INTRODUCTION

Solar energetic particles (SEPs) are charged energetic particles occasionally emitted by the Sun during its burst events. Generally, SEPs are produced by solar flares or/and related to coronal mass ejections (CMEs), although the relative importance of flares and CME-driven shocks in producing high-energy particles is not completely understood. The propagation of SEPs in the heliosphere remains one of the important subjects of space physics, heliophysics, and plasma physics. In addition, large solar proton events (SPEs) significantly affect the solar-terrestrial space environment, and thereby have become an important topic in the research fields of space radiation, space weather, and space climate. Recently, multi-spacecraft observations (STEREO-A/B, ACE, SOHO, Wind, etc.) and three-dimensional transport modeling have been intensely used in the studies of SEP events.

Essentially, the propagation of SEPs in interplanetary space includes several fundamental physical mechanisms, such as particle streaming along magnetic field lines, convection with the solar wind, adiabatic magnetic focusing, pitch-angle diffusion, adiabatic cooling, and perpendicular diffusion. According to the well-known quasi-linear theory for cosmic ray diffusion (Jokipii 1966), the perpendicular diffusion coefficient is usually much smaller than the parallel diffusion coefficient. Therefore, the effects of perpendicular diffusion were often ignored in previous theoretical, numerical, and observational studies of SEP propagation. However, the observations of SEP events detected by the Helios mission proposed some nonlinear effects near 90° pitch angle of particles (e.g., Hasselmann & Wibberenz 1968, 1970; Beeck & Wibberenz 1986; Beeck et al. 1987). Further investigations showed that when the magnetic turbulence is quite strong, the perpendicular diffusion could be comparable to the parallel diffusion (e.g., Shalchi 2005). Recently, with the launch of the twin spacecraft STEREO-

⋆ E-mail: hqhe@mail.iggcas.ac.cn

© 2016 The Authors

A/B and the development of three-dimensional transport modeling, the significant role of perpendicular diffusion in the SEP propagation has become gradually and increasingly well known in the SEP community. The important effects of perpendicular diffusion on SEP transport and distribution in the heliosphere were found in both numerical modeling studies and observational studies (e.g., Zhang et al. 2009; He et al. 2011; He & Wan 2015; He 2015; Dröge et al. 2010, 2014; Dresing et al. 2012, 2014; Giacalone & Jokipii 2012; Strauss & Fichtner 2015). Note that the diffusion could not only be anisotropic with respect to the directions perpendicular and parallel to the magnetic field, but that it could also be fully anisotropic. For example, the case of two different perpendicular diffusion coefficients has been discussed in Effenberger et al. (2012), and also applied to SEPs by Kelly et al. (2012). In the sense of perpendicular diffusion, some interesting SEP phenomena were reproduced or found by performing complete model calculations of SEP propagation in the three-dimensional interplanetary magnetic field with the effects of turbulence (for a recent brief review, see He 2015).

In previous simulation works, it was found that with the same heliographic longitude separation between the magnetic footpoint of the observer and the solar sources, the SEPs associated with the sources located at east are detected earlier and with larger fluxes than those associated with the sources located at west (He et al. 2011; He & Wan 2015). This SEP phenomenon was called the "East-West azimuthal asymmetry" by He et al. (2011). In this work, we focus on the so-called East-West azimuthal asymmetry of SEPs in view of statistical analysis of solar proton events. We mainly pay attention to the relatively longitudinal distribution of solar proton events. The longitudinally asymmetric distribution phenomenon of solar proton events is found. With the same longitudinal separation between magnetic footpoint of observer and solar sources, the number of the SPEs originating from sources located on the eastern side of the magnetic footpoint of observer is larger than the number of the SPEs from sources located on the western side. Essentially, this observational result is consistent with our previous numerical simulation results. We further discuss in detail the physical mechanism responsible for this SEP phenomenon in two scenarios, i.e., "multiple SEP events with one spacecraft" and "one SEP event with multiple spacecraft". The effects of perpendicular diffusion on the heliospheric propagation and the East-West longitudinally (azimuthally) asymmetric distribution of SEPs are emphasized in the discussions. We also compare our statistical and numerical results with the observational study of Dresing et al. (2014). In the context of perpendicular diffusion, our results and those of Dresing et al. (2014) are unified and identified with each other.

This paper is structured as follows. In Section 2, we briefly describe the collected data set of 78 solar proton events accumulated during 1996-2011, based on which the statistical analysis will be carried out. In Section 3, we present the statistical results of the 78 solar proton events. In Section 4, we discuss the physical mechanism responsible for the East-West longitudinal (azimuthal) asymmetry of SEP distribution in the heliosphere. The important effects of perpendicular diffusion will be discussed in detail. The inherent relationship between our works and other statistical survey of SEP events (Dresing et al. 2014) will be discussed in Section 5. A summary of our results will be provided in Section 6.

2 SOLAR PROTON EVENTS ANALYZED IN THIS INVESTIGATION

The 78 solar proton events affecting the Earth environment detected during 1996-2011 are collected from Space Weather Prediction Center of National Oceanic and Atmospheric Administration (NOAA). The solar proton events and associated flares and CMEs are listed in Table A1. The maximum intensity of each solar proton event for energies > 10 MeV is larger than 10 particle flux units (pfu). Note that 1 pfu=1 particles/$(cm^2 - sr - s)$. We also note that the 78 solar proton events presented in Table A1 are collected from the original listing by excluding the events without identifiable origin location on the solar surface. The SEP events without definite source location are randomly distributed on the solar surface, i.e., the SEP events excluded from the listing may locate on either the eastern or the western side of the solar surface.

The first three columns in Table A1 give the start time, maximum time, and proton flux of each SEP event, respectively. The main direction and onset time of CME associated with each particle event are listed in Column 4. Columns 5 and 6 provide the maximum time and importance (X ray/optical) of flare associated with each SEP event. The majority of the SEP events presented in Table 1 were observed at the onset of the solar events. Generally, intense SEP events are usually associated with both major flares and large CMEs, and consequently, the relative roles of flares and CME-driven shocks in producing high-energy particles are not completely understood (Cliver & Cane 2002). In addition, most of the SEPs in impulsive events are released near the surface of the Sun. Even in many gradual events, energetic particles, particularly those with high energies, are generated near the Sun, where the shock is very fast, the magnetic field is quite strong and the seed particles are dense (Zhang et al. 2009). Therefore, in the investigation, we do not particularly discriminate between the two types of particle sources. The location and number of each associated active region are listed in columns 7 and 8, respectively. The last three columns in Table A1 provide the solar wind speeds measured by spacecraft Solar and Heliospheric Observatory (SOHO), ACE, and the mean value of them, respectively. By averaging SOHO or ACE data measured in the time interval $[T_{max} - 2hr, T_{max} + 2hr]$, in which T_{max} indicates the maximum time of the corresponding SEP event, we can obtain the solar wind speed in each SEP event. The averaged solar wind speed will be used in our statistical investigation. As one can see, for some solar proton events, only the SOHO data of solar wind speeds are available, and for some events, only the ACE data are available. Moreover, if there are not valid solar wind speed data in the time range $[T_{max} - 2hr, T_{max} + 2hr]$ for a certain solar proton event, the averaged solar wind speed obtained from the complete observational data on the whole day when the maximum of the event occurred will be used. In addition, we note that the solar wind speed 790 $km\ s^{-1}$ during the 2003 October

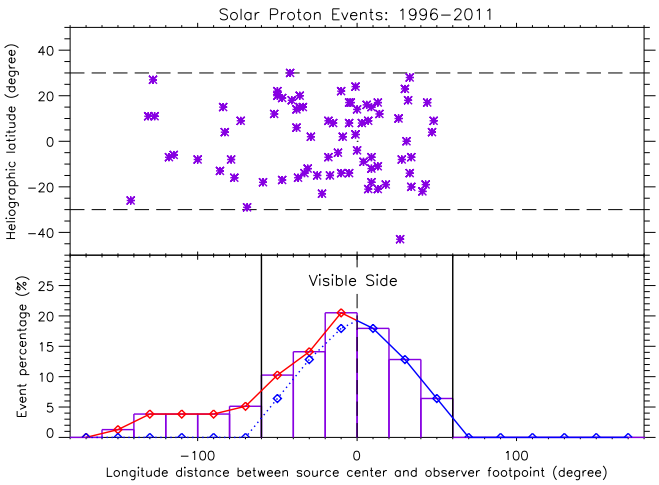
Solar Proton Events: 1996−2011
Heliographic latitude (degree)
Visible Side
Event percentage (%)
Longitude distance between source center and observer footpoint (degree)

Figure 1. Spatial distribution of the solar sources of 78 solar proton events observed near the Earth's orbit during 1996-2011. Upper panel: latitudinal and longitudinal distribution. Lower panel: number percentage distribution of the solar events along the relative longitude ϕ_r. Adapted from Figure 1 of He & Wan (2013).

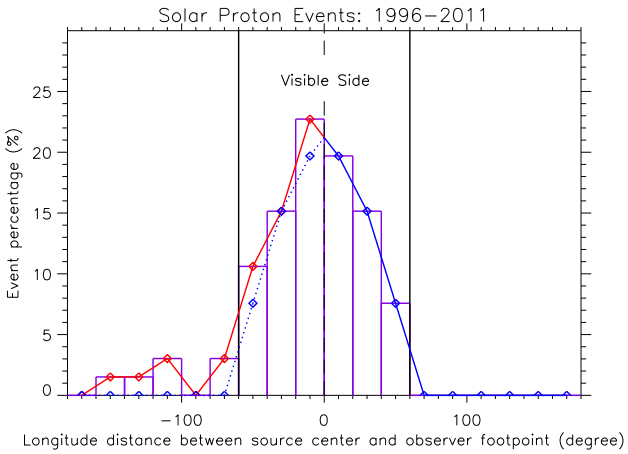
Solar Proton Events: 1996−2011
Visible Side
Event percentage (%)
Longitude distance between source center and observer footpoint (degree)

Figure 2. Number percentage distribution of the solar sources of the 66 SEP events with relatively short delays along the relative longitude ϕ_r. With the same longitudinal distance between the observer's magnetic footpoint and solar sources, the number of the SEP events originating from sources located on the eastern (left) side of the observer's footpoint is larger than the number of the SEP events from sources located on the western (right) side.

28 solar proton event listed in Table A1 is adopted from Veselovsky et al. (2004).

In the investigation, we utilize the solar wind speeds according to the rules as: if both of the solar wind speeds obtained from SOHO and ACE data, respectively, are available, then we employ the mean value of them, i.e., $\overline{V}^{sw} = (V^{sw}_{soho} + V^{sw}_{ace})/2$, where V^{sw}_{soho} and V^{sw}_{ace} are the solar wind speeds averaged from SOHO and ACE data, respectively; otherwise, the solar wind speed derived from the measurements by a single spacecraft (SOHO or ACE) will be used.

3 EAST-WEST AZIMUTHAL ASYMMETRY OF SOLAR PROTON EVENTS

The rotation angle of the nominal interplanetary magnetic field line connecting the observer at radial distance r with the Sun can be calculated through this expression (e.g., Parker 1958)

$$\phi_s = \Omega r / V^{sw}. \quad (1)$$

Here, Ω indicates the Sun's angular rotation rate, r indicates the heliocentric radial distance, and V^{sw} indicates the solar wind speed. Note that the nominal magnetic footpoint of the spacecraft calculated through the above expression may differ from the actual footpoint, since sometimes the deviations of the interplanetary magnetic field can be significant. But in the statistical sense, this will not affect our main results. The west and east heliographic longitudes ϕ of the solar sources are usually indicated by positive and negative values, respectively. The relative longitude ϕ_r between the solar flare and the observer's magnetic footpoint can be obtained via this relation

$$\phi_r = \phi - \Omega r / V^{sw}. \quad (2)$$

According to the realistic solar wind speed measured by the spacecraft, we can obtain the relative longitude ϕ_r for each solar proton event listed in Table A1.

We present the statistical result of the solar proton events in Figure 1. A preliminary result was reported in He & Wan (2013). In the upper panel, it can be seen that the solar flares are primarily distributed within $[S30°, N30°]$, which is consistent with the result in Zhao et al. (2007). We divide the relative longitude ϕ_r into bins: $[-180°, -160°]$, $[-160°, -140°]$, ..., $[160°, 180°]$. The number percentage distribution of the solar events along the relative longitude ϕ_r is presented in the lower panel. We note that the negative value (left) and positive value (right) indicate that the solar flares locate on the eastern side and western side of the magnetic footpoint of observer, respectively. To directly compare the event number percentages between the east and west relative longitude, the event number percentages on the right side are mirrored to the left side, indicated by a blue dotted line. We mainly pay attention to the central longitude range of the visible side of the Sun, as indicated between the two vertical lines in Figure 1. It can be seen that with the same longitudinal separation between the magnetic footpoint of observer and solar sources, the number of the solar proton events originating from sources located on the eastern side of the observer's magnetic footpoint is larger than the number of the solar proton events from sources located on the western side (He & Wan 2013).

Generally, a SEP event which starts with a long delay at the observer is more possibly related to a CME-driven shock. So we further collect 66 SEP events from Table A1 by excluding the events with a delay of more than 24 hours with respect to the flare maximum. We also statistically investigate the number percentage distribution of these 66 SEP events along the relative longitude ϕ_r. Figure 2 shows the statistical results. We also pay attention to the central longitude range of the visible side of the Sun. As we can see, the number percentage of the SEP events on the left side is generally larger than that on the right side, similar to the results in Figure 1. As noted above, most of the high-energy SEPs (associated with either flares or CME-driven shocks) are probably produced near the Sun. After the SEPs are released on or near the Sun, they will transport in the inter-

planetary magnetic field with turbulence. During the transport processes in the heliosphere, the parallel diffusion and perpendicular diffusion play a very important role in the SEP distribution and anisotropy. Therefore, we note that even for CME-associated SEP events, the East-West longitudinal (azimuthal) asymmetry of SEP distribution, due to the effects of perpendicular diffusion, will hold. In this sense, it is not very necessary to particularly discriminate between the two types of SEP sources, i.e., solar flares and CME-driven shocks. Actually, the traditional classification paradigm of the so-called impulsive and gradual SEP events is increasingly challenged by the current multi-spacecraft observations (STEREO-A/B, ACE, SOHO, Wind, etc.) and the numerical modeling of three-dimensional focused transport of SEPs.

4 DISCUSSIONS ON THE MECHANISM RESPONSIBLE FOR EAST-WEST AZIMUTHAL ASYMMETRY OF SEPS

Our previous numerical simulations of SEP transport with the effect of perpendicular diffusion demonstrated that there exists an East-West longitudinal (azimuthal) asymmetry both in the entire intensities and in the peak intensities of SEPs transporting in the interplanetary space (see He et al. 2011; He & Wan 2013, 2015). As pointed out by these works, the longitudinally (azimuthally) asymmetric distribution of SEPs results from the East-West azimuthal asymmetry in the geometry of the Parker interplanetary magnetic field as well as the effects of perpendicular diffusion on the transport processes of SEPs in the heliosphere. The formation mechanism of the East-West longitudinal (azimuthal) asymmetry of SEP distribution via perpendicular diffusion is sketched in Figure 3, which is referred to the physical scenario of "multiple SEP events with one spacecraft". The SEP transport in the interplanetary magnetic field mainly includes the parallel diffusion and the perpendicular diffusion. Due to the effect of the perpendicular diffusion, the SEPs released from acceleration regions with limited coverage can cross the interplanetary magnetic field lines and transport to distant heliospheric locations with very wide longitudinal or/and latitudinal separations. In Figure 3, the intensity of SEPs (detected at spacecraft's position O_2) originating from solar source A (as an example) located on the eastern side of the observer footpoint is nearly equivalent to the SEP intensity at position A_1, in a statistical sense. Similarly, the intensity of SEPs (detected at spacecraft's position O_2) released from solar source B (with the same longitudinal separation as source A relative to the observer footpoint) located on the western side is nearly equivalent to the SEP intensity at position B_1, in a statistical sense. As one can see, the heliocentric radial distance $\overline{OA_1}$ between solar center (O) and the position A_1 is shorter than that $\overline{OB_1}$ between solar center (O) and the position B_1. Note that the extent of the length difference between the heliocentric radial distances $\overline{OA_1}$ and $\overline{OB_1}$ depends on the longitudinal separation between the sources and the observer's footpoint. Specifically, a larger longitudinal separation leads to a more significant length difference between the radial distances of the east and west equivalent positions (e.g., A_1 and B_1 in Figure 3).

Observational analysis showed that the peak intensities

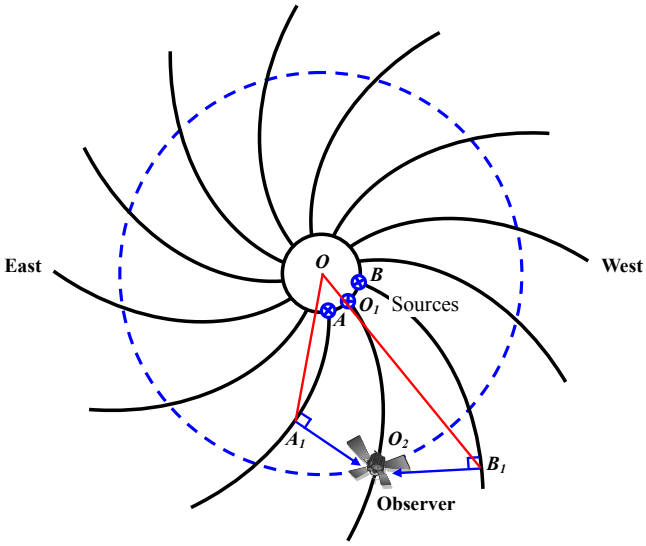

Figure 3. Diagram to illustrate the formation of the East-West longitudinal (azimuthal) asymmetry of SEP distribution via perpendicular diffusion in the physical scenario of "multiple SEP events with one spacecraft". In a statistical sense, the intensity of SEPs (detected at position O_2) originating from solar source A (B) located on the eastern (western) side of the observer footpoint is nearly equivalent to the SEP intensity at position A_1 (B_1). The heliocentric radial distance $\overline{OA_1}$ between solar center (O) and the position A_1 is shorter than that $\overline{OB_1}$ between solar center (O) and the position B_1.

of SEPs decrease with the heliocentric radial distance (r) in a functional form of $r^{-\alpha}$, with α varying in a wide range. Basically, our numerical modeling of the five-dimensional Fokker-Planck transport equation has confirmed these observational results. In this paper, we present a numerical modeling result in Figure 4 regarding radial dependence of intensity-time profiles and peak intensities of SEPs observed along the nominal Parker magnetic field line connecting the spacecraft with the solar source. The upper panel of Figure 4 presents the intensity-time profiles of 32 MeV protons observed at different heliocentric radial distances: 0.25, 0.4, 0.6, 0.8, and 1.0 AU. Both the solar source and the observers are located at 90° colatitude in this typical case study. As one can see, during the entire evolution process, the particle intensity observed at a smaller radial distance is higher than the particle intensity detected at a larger radial distance.

In addition, we can obviously see that during the late phase, the intensity-time profiles of all the SEP cases display nearly the same decay rate, which is known as the SEP reservoir phenomenon in spacecraft observations (e.g., Roelof et al. 1992). Therefore, our simulations of a series of SEP cases with different radial distances reproduce the so-called SEP reservoir phenomenon. Actually, our numerical simulations with perpendicular diffusion reproduced various SEP reservoirs at different heliospheric locations (longitude, latitude, and radial distance) without invoking the prevailing hypothesis of a reflecting boundary (magnetic mirror) or diffusion barrier (solar wind structure) (e.g., He et al. 2011; He & Wan 2015; He 2015). Additionally, so far no any explicit observational evidence or quantitative description of reflecting boundaries (magnetic mirrors) or diffusion barriers (solar wind structures), which were once prevalently

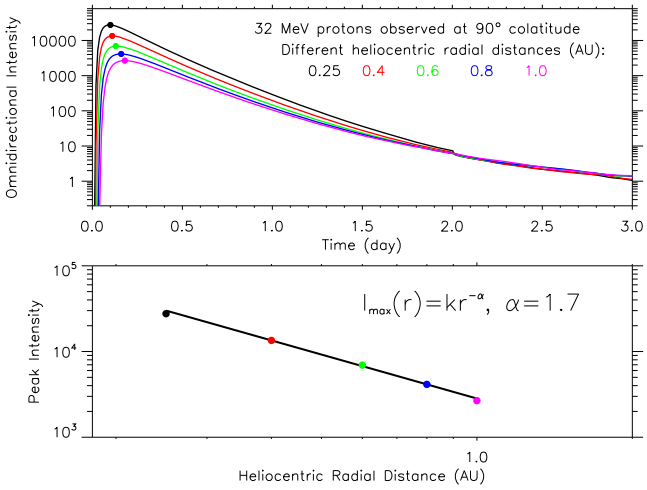

Figure 4. Simulated radial dependence of intensity-time profiles and peak intensities of SEPs observed along the nominal Parker magnetic field line connecting the solar source. Upper panel: The intensity-time profiles of 32 MeV protons observed at different radial distances: 0.25, 0.4, 0.6, 0.8, and 1.0 AU. Both the solar source and the observers are located at 90° colatitude. Note that the so-called SEP reservoir phenomenon is reproduced in the simulations of a series of SEP cases with different radial distances. Lower panel: The radial dependence of the SEP peak intensities extracted from the intensity-time profiles shown in the upper panel. A functional form of $I_{max}(r) = kr^{-\alpha}$ with index $\alpha = 1.7$ is obtained.

supposed to exist in the heliosphere to contain the particles long enough to form the observed SEP reservoirs, has been provided or specified within the community (for discussions, see He 2015). Actually, as He & Wan (2015) and He (2015) pointed out, it is difficult to imagine such an "overwhelming" reflecting boundary (magnetic mirror) or diffusion barrier (solar wind structure) covering all of the longitudes, all of the latitudes, and even all of the radial distances, and even exactly accompanying almost all of the SEP events including the so-called impulsive or ^{3}He-rich events. Therefore, in the sense of perpendicular diffusion, we suggest that the so-called SEP "reservoir" should be renamed SEP "flood", which is more appropriate to illustrate the transport processes of SEPs in the heliosphere.

In the upper panel of Figure 4, the filled circles with different colors on the intensity-time profiles denote the peak intensities of the corresponding SEP cases. We extract the information of the peak intensities and the relevant radial distances in the SEP cases, and present it in the lower panel of Figure 4. We further model the radial dependence of the peak intensities I_{max} with a power-law function $I_{max}(r) = kr^{-\alpha}$, where k is a constant in this case study. We obtain the power-law index $\alpha = 1.7$ in this series of SEP cases. We note that the index α mainly depends on the properties (e.g., coverage, location) of SEP sources and the relative locations of magnetic field line footpoints of the observers. From the lower panel of Figure 4, we can clearly see that the peak particle intensities of SEP events exponentially decrease with the increasing radial distances.

According to the relationship $\overline{OA_1} < \overline{OB_1}$ sketched in Figure 3 and the radial dependence of SEP peak intensities $I_{max}(r) = kr^{-\alpha}$ with, e.g., $\alpha = 1.7$ in this work, we can readily deduce that the peak intensity observed at position A_1 is larger than that observed at position B_1. Actually as shown in the upper panel of Figure 4, the SEP intensity detected at position A_1 is larger than that detected at position B_1 through the whole evolution process. We also note that these results are valid for arbitrary energies of energetic particles and for arbitrary particle species including electrons and heavy ions. Therefore, the particle fluence and radiation dose received at position A_1 are, respectively, higher than those received at position B_1. Then according to the intensity equivalence relationship discussed above between A_1 and O_2 (observing SEPs from source A) as well as that between B_1 and O_2 (observing SEPs from source B), we can infer that the entire intensity, peak intensity, particle fluence, and radiation dose originating from source A are, respectively, larger than those originating from source B. We note that these conclusions hold for arbitrary couple of solar sources located on the eastern and western sides of the observer's magnetic footpoint, respectively, but with the same longitudinal separation relative to the observer's magnetic footpoint.

In typical cases of interplanetary conditions, the perpendicular diffusion coefficient should be smaller than the parallel diffusion coefficient, as performed in our previous numerical modeling, although the effect of perpendicular diffusion always plays a very important role in the transport and distribution of SEPs. Therefore, we note that the longitudinal separation between the source region and the magnetic footpoint of the observer is the most crucial factor in determining the longitudinal variation of the entire intensity and the peak intensity of SEPs, indicating that the farther the magnetic footpoint of the observer is away from the solar source, the smaller the SEP intensity will be observed by the spacecraft and also the later the SEP event onset will be detected.

The probability of an SEP event being detected by spacecraft in the interplanetary space is related to the SEP intensity in the event and the detection threshold of the instruments onboard the spacecraft. In addition, note that the criterion of an event being recorded in the SPE listing of NOAA is that the flux of the event being larger than or equal to 10 pfu. Therefore, the spacecraft detection threshold and SPE listing criterion naturally play a role in the historical records of SEP events affecting the Earth environment. Our previous simulations showed that with the same longitudinal separations between the solar sources and the magnetic footpoint of the observer, the SEP events originating from solar sources on the eastern side of the magnetic footpoint of the observer reveal larger fluxes than those from solar sources on the western side (He et al. 2011; He & Wan 2015). Therefore, the SEP events from solar sources on the eastern (western) side of observer's magnetic footpoint will have a larger (smaller) probability of being detected and recorded by spacecraft near the Earth's orbit. When a large data set of SEP events is taken into account, it is natural and expectable to obtain the East-West longitudinal (azimuthal) asymmetry (Figures 1 and 2). As discussed above, the detection threshold and listing criterion naturally play a role in the statistical results of the East-West longitudinally (azimuthally) asymmetric distribution of SEP events. We point out that no matter what the detection threshold (e.g., particle flux, particle energy, particle species, etc.) or listing

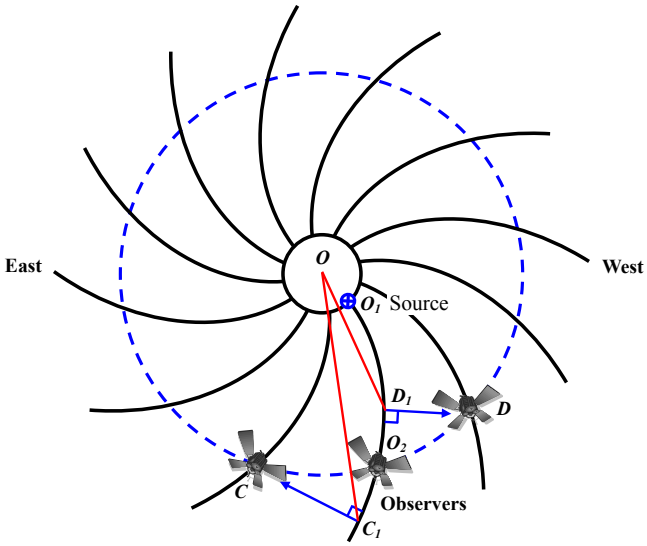

Figure 5. Diagram to illustrate the formation of the East-West longitudinal (azimuthal) asymmetry of SEP distribution via perpendicular diffusion in the physical scenario of "one SEP event with multiple spacecraft". In a statistical sense, the SEP intensity observed by spacecraft D (C) located on the western (eastern) side is nearly equivalent to the SEP intensity observed at position D_1 (C_1). The heliocentric radial distance $\overline{OD_1}$ between solar center (O) and the position D_1 is smaller than that $\overline{OC_1}$ between solar center (O) and the position C_1.

criterion is, the result of the East-West longitudinal (azimuthal) asymmetry of SEP events will hold, provided that a relatively large data set is taken into account. We emphasize that our numerical simulations of five-dimensional transport equation and statistical analysis of SEP events confirm each other. Furthermore, the combination of statistical survey and numerical modeling regarding the East-West longitudinal (azimuthal) asymmetry presents a unique evidence for the effects of perpendicular diffusion on the SEP propagation in the heliosphere.

5 RELATIONSHIP BETWEEN OUR RESULTS AND THOSE OF A RECENT WORK

In a recent work (Dresing et al. 2014), the authors also presented a statistical survey of the longitudinal distribution of SEP peak intensities observed by twin spacecraft STEREO-A/B and near-Earth spacecraft ACE. A similar investigation of SEP peak intensities can be found in Lario et al. (2013), where the SEP intensity asymmetry was also presented. Essentially, their results, obtained in a "one SEP event with multiple spacecraft" style, are consistent with and confirm our numerical modeling and observational results. In this section, we discuss the relationship between our results and those of Dresing et al. (2014).

Figure 5 sketches the physical scenario of the multi-spacecraft observations of SEPs originating from a common particle source (e.g., source O_1) on the solar surface. The three spacecraft (marked with C, O_2, and D, respectively, from East to West) are located at heliospheric positions with the same heliocentric radial distance but with different heliolongitudes. Specifically, the spacecraft O_2 in the middle is directly connected to the solar source O_1 by the interplanetary magnetic field line, whereas the magnetic footpoints of the spacecraft C on the left and spacecraft D on the right are located on the eastern side and western side, respectively, with the same longitudinal separation, relative to the solar source O_1. After being released from the solar surface, the energetic particles will transport diffusively in turbulent interplanetary magnetic field, consisting of parallel diffusion along and perpendicular diffusion across the mean magnetic field. Due to the effects of perpendicular diffusion, the energetic particles released from a solar source (e.g., source O_1) with limited coverage can be detected by multiple spacecraft with wide longitudinal or/and latitudinal separations between every couple of them. The SEP intensity observed by spacecraft D located on the western side is nearly equivalent to the SEP intensity observed at position D_1, in a statistical sense. Likewise, the SEP intensity detected by spacecraft C located on the eastern side is nearly equivalent to the SEP intensity detected at position C_1, in a statistical sense. As we can see, the heliocentric radial distance $\overline{OD_1}$ between solar center (O) and the position D_1 is smaller than that $\overline{OC_1}$ between solar center (O) and the position C_1. Note that the extent of the length difference between the radial distances $\overline{OC_1}$ and $\overline{OD_1}$ depends on the longitudinal separation between the source and the observer footpoints. A larger longitudinal separation leads to a more considerable length difference between the radial distances $\overline{OC_1}$ and $\overline{OD_1}$. In combination with the numerical simulation result of the radial dependence of SEP intensity-time profiles and SEP peak intensities ($I_{max}(r) = kr^{-\alpha}$) as shown in Figure 4 and discussed above, we can readily infer that the SEP intensity (both entire intensity and peak intensity) observed at position D_1 is larger than that observed at position C_1. According to the intensity equivalence relationship between positions D and D_1 as well as that between positions C and C_1, we can infer that the SEP intensity (both entire intensity and peak intensity) observed by the western spacecraft D is larger than that observed by the eastern spacecraft C. As a natural result of interplay between perpendicular diffusion and parallel diffusion, the observation location of the highest intensity-time profile and the largest peak intensity of SEPs will shift from the place of best magnetic connection and slightly toward the west of the associated SEP source. We note that these results are valid for arbitrary energies of energetic particles and for arbitrary particle species including electrons and heavy ions.

Figure 6 presents the relationship between our physical scenario and that of Dresing et al. (2014). The SEP sources A and B and spacecraft O_2 labeled in blue indicate the "multiple SEP events with one spacecraft" scenario, and the SEP source O_1 and spacecraft C and D labeled in red indicate the "one SEP event with multiple spacecraft" scenario. We emphasize the importance of the concept of "relative position" in understanding the physical relationship between our results and those of Dresing et al. (2014). As shown in Figure 6, the relative position between SEP source A and spacecraft O_2 is equivalent to the relative position between source O_1 and spacecraft D; the relative position between source B and spacecraft O_2 is equivalent to the relative position between source O_1 and spacecraft C. Therefore, the intensity observed by spacecraft O_2 of SEPs originating from source A is equivalent to the intensity observed by space-

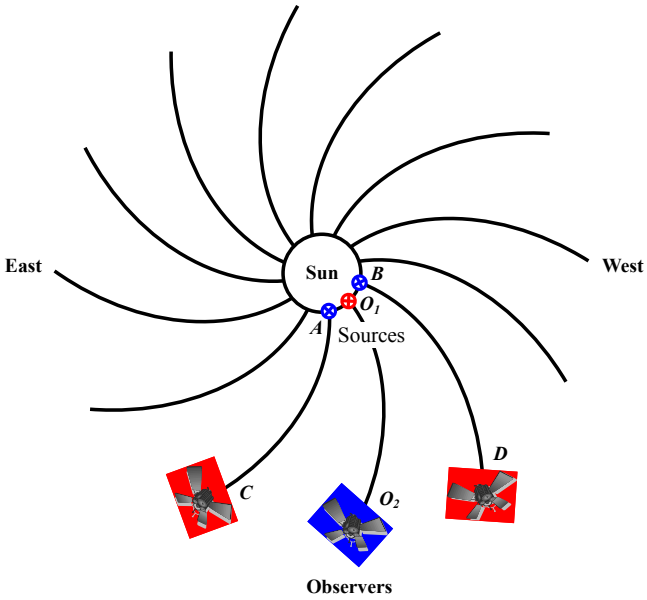

Figure 6. Diagram to illustrate the relationship between the two physical scenarios of "multiple SEP events with one spacecraft" (sources A and B and spacecraft O_2 labeled in blue) and "one SEP event with multiple spacecraft" (source O_1 and spacecraft C and D labeled in red). The relative position between source A (B) and spacecraft O_2 is equivalent to the relative position between source O_1 and spacecraft D (C). With this "spiral transformation trick", the two physical scenarios are unified and identified with each other.

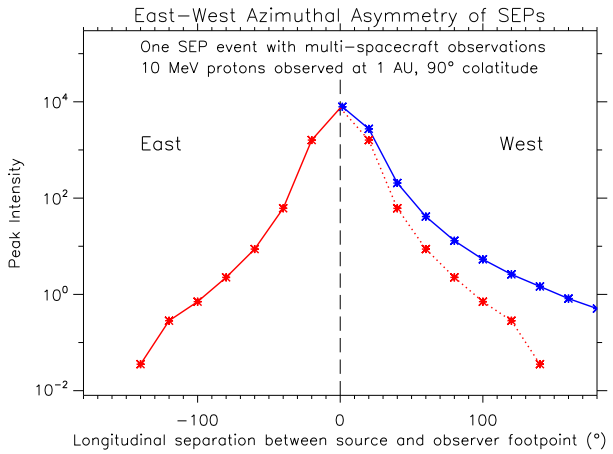

Figure 7. Multidimensional numerical modeling of the East-West longitudinal (azimuthal) asymmetry of SEP distribution in the scenario of "one SEP event with multiple spacecraft". The red (blue) solid line on the left (right) indicates the peak intensities of 10 MeV protons observed by spacecraft located at the eastern (western) side of the solar source. The red dotted line on the right is mirrored from the left. It can be clearly seen that the SEP peak intensities observed by spacecraft located at the western side of the SEP source are systematically larger than those observed by spacecraft located at the eastern side. In addition, the location of the largest SEP peak intensity slightly shifts to the west of the SEP source.

craft D of SEPs originating from source O_1; the intensity observed by spacecraft O_2 of SEPs originating from source B is equivalent to the intensity observed by spacecraft C of SEPs originating from source O_1. Accordingly, with the same longitudinal separation between the solar source and the magnetic footpoint of the observer, the following two results are essentially the same: (1) in the scenario of "multiple SEP events with one spacecraft", the SEP intensity originating from the solar source (e.g., source A in Figure 6) located at the eastern side of observer footpoint is larger than the SEP intensity originating from the source (e.g., source B) located at the western side; (2) in the scenario of "one SEP event with multiple spacecraft", the SEP intensity observed by the spacecraft (e.g., spacecraft D) located at the western side of the SEP source is larger than the SEP intensity detected by the spacecraft (e.g., spacecraft C) located at the eastern side. By performing such "spiral transformation trick" as shown in Figure 6, the two physical scenarios presented in our works (He et al. 2011; He & Wan 2013, 2015) and in Dresing et al. (2014) are essentially unified and identified with each other.

As an example, Figure 7 presents the multidimensional numerical modeling result of the East-West longitudinal (azimuthal) asymmetry of SEPs in the scenario of "one SEP event with multiple spacecraft". For more details on the numerical model and numerical method of the five-dimensional Fokker-Planck focused transport equation, we refer the reader to our simulation works (e.g., He et al. 2011; He & Wan 2015; He 2015). In this work, we only present Figure 7 to demonstrate the relationship between our results and those of Dresing et al. (2014). The red solid line on the left-hand half in Figure 7 indicates the peak intensities of 10 MeV protons observed by a series of spacecraft located at the eastern side of the nominal magnetic field line connecting the solar source. On the right-hand half of Figure 7, the blue solid line indicates the peak intensities of 10 MeV protons detected by a series of spacecraft located at the western side of the nominal field line connecting the SEP source. For direct comparison between the two halves, we further mirror the SEP peak intensities from the left-hand half to the right-hand half with a red dotted line. After this operation, we can clearly see that the SEP peak intensities observed by spacecraft located at the western side of the SEP source are systematically larger than those observed by spacecraft located at the eastern side. According to the discussions above and our numerical simulations, actually, during the entire evolution process, the SEP intensity observed at the western side is larger than that observed at the eastern side, provided that the magnetic footpoints of the pair of observers located at the western and eastern sides, respectively, are with the same longitudinal separation relative to the SEP source. In addition, due to the interplay between perpendicular diffusion and parallel diffusion, the longitudinal location at which the largest SEP peak intensity is observed slightly shifts to somewhere on the western side of the SEP source. Basically, the accurate extent of west-shift depends on the ratio of perpendicular to parallel diffusion coefficients, geometry of the Parker magnetic spiral (corresponding to solar wind speed), particle energy and species, coverage of the SEP sources, and particle spatial distribution in the sources.

6 SUMMARY AND CONCLUSIONS

He et al. (2011) reported that with the same longitudinal separation between magnetic footpoint of observer and SEP sources, the SEPs produced from the sources located east are detected earlier with higher fluxes than those associated with the sources located west (see also He & Wan 2013, 2015). Our statistical survey of solar proton events showed that with the same longitudinal separation between the observer's magnetic footpoint and the SEP sources, the number of SEP events associated with the sources located on the eastern side of the observer's magnetic footpoint is larger than the number of the SEP events originating from the sources located on the western side. Generally, the probability of a solar proton event being observed by spacecraft in the interplanetary space depends on the SEP intensity in the event as well as the instrumental sensitivity threshold of the spacecraft. Therefore, our statistical analysis of SEP events accumulated over 16 years and our numerical simulations of the five-dimensional Fokker-Planck transport equation modeling taking into account perpendicular diffusion confirm each other. We further point out that the statistical results of solar proton events accumulated over a long time period provide an observational evidence for the effects of perpendicular diffusion on the SEP propagation in the interplanetary space.

We discuss in detail the effects of perpendicular diffusion on the formation of the East-West longitudinally (azimuthally) asymmetric distribution of SEPs. The role of perpendicular diffusion in the physical scenarios of both "multiple SEP events with one spacecraft" and "one SEP event with multiple spacecraft" is thoroughly demonstrated. We obtain the radial dependence of SEP peak intensities $I_{max}(r) = kr^{-1.7}$ from numerically modeling the five-dimensional Fokker-Planck focused transport equation. We employ this functional relation ($I_{max}(r) = kr^{-1.7}$) to quantitatively illustrate and explain the East-West longitudinal (azimuthal) asymmetry of SEP distribution in the heliosphere. The inherent relationship between our results (He et al. 2011; He & Wan 2013, 2015) and those of Dresing et al. (2014) is comprehensively discussed. In the context of perpendicular diffusion, our results and those of Dresing et al. (2014) are essentially unified and identified with each other. We note that the SEP phenomenon of longitudinally (azimuthally) asymmetric distribution ("East-West azimuthal asymmetry") cannot be decently explained by any other hypothetical mechanisms including the so-called reflecting boundary (magnetic mirror) and diffusion barrier (solar wind structure).

In this work, we primarily discuss the SEP scenario in the ecliptic plane. It should be noted that the results and the conclusions presented above essentially hold for arbitrary heliospheric latitudes. As a special and unique SEP phenomenon, the East-West longitudinally (azimuthally) asymmetric distribution of SEPs represents the important effects of the perpendicular diffusion processes (which was usually ignored in previous studies, especially in the observational community) and of the large-scale Parker spiral geometry of the interplanetary magnetic field. In addition, we note that the East-West longitudinal (azimuthal) asymmetry of SEP distribution is a universal phenomenon independent of particle energy, particle species, particle origin (on or near the Sun or in the interplanetary space), and observer's location (latitude, longitude, and radial distance) in the heliosphere. Therefore, our results presented in this work will be valuable for understanding the Sun-Earth relations and especially for understanding the three-dimensional propagation of SEPs in the heliosphere.

ACKNOWLEDGEMENTS

This work was supported in part by the National Natural Science Foundation of China under grants 41204130, 41474154, 41321003, and 41131066, the National Important Basic Research Project under grant 2011CB811405, the Chinese Academy of Sciences under grant KZZD-EW-01-2, and the Open Research Program from Key Laboratory of Geospace Environment, Chinese Academy of Sciences. H.-Q. He gratefully acknowledges the partial support of the International Postdoctoral Exchange Fellowship Program of China under grant 20130023, and the K. C. Wong Education Foundation. We benefited from the solar proton events data provided by the Space Weather Prediction Center of NOAA and the instrument teams of GOES spacecraft. We thank the NASA/Space Physics Data Facility (SPDF)/CDAWeb for providing the solar wind data of SOHO and ACE.

REFERENCES

Beeck, J., & Wibberenz, G. 1986, ApJ, 311, 437
Beeck, J., Mason, G. M., Hamilton, D. C., et al. 1987, ApJ, 322, 1052
Cliver, E. W., & Cane, H. V. 2002, EOS Trans. AGU, 83, 61
Dresing, N., Gómez-Herrero, R., Heber, B., et al. 2014, A&A, 567, A27
Dresing, N., Gómez-Herrero, R., Klassen, A., Heber, B., Kartavykh, Y., & Dröge, W. 2012, Sol. Phys., 281, 281
Dröge, W., Kartavykh, Y. Y., Dresing, N., Heber, B., & Klassen, A. 2014, J. Geophys. Res., 119, 6074
Dröge, W., Kartavykh, Y. Y., Klecker, B., & Kovaltsov, G. A. 2010, ApJ, 709, 912
Effenberger, F., Fichtner, H., Scherer, K., et al. 2012, ApJ, 750, 108
Giacalone, J., & Jokipii, J. R. 2012, ApJ, 751, L33
Hasselmann, K., & Wibberenz, G. 1968, Z. Geophys., 34, 353
Hasselmann, K., & Wibberenz, G. 1970, ApJ, 162, 1049
He, H.-Q., Qin, G., & Zhang, M. 2011, ApJ, 734, 74
He, H.-Q., & Wan, W. 2013, Proc. ICRC (Brazil), paper 0267, arXiv:1502.03090
He, H.-Q., & Wan, W. 2015, ApJS, 218, 17
He, H.-Q. 2015, ApJ, 814, 157
Jokipii, J. R. 1966, ApJ, 146, 480
Kelly, J., Dalla, S., & Laitinen, T. 2012, ApJ, 750, 47
Lario, D., Aran, A., Gómez-Herrero, R., et al. 2013, ApJ, 767, 41
Parker, E. N. 1958, ApJ, 128, 664
Roelof, E. C., Gold, R. E., Simnett, G. M., Tappin, S. J., Armstrong, T. P., & Lanzerotti, L. J. 1992, Geophys. Res. Lett., 19, 1243
Shalchi, A. 2005, MNRAS, 363, 107
Strauss, R. D., & Fichtner, H. 2015, ApJ, 801, 29
Veselovsky, I. S., Panasyuk, M. I., Avdyushin, S. I., et al. 2004, Cosmic Research, 42, 435
Zhang, M., Qin, G., & Rassoul, H. 2009, ApJ, 692, 109
Zhao, X., Feng, X., & Wu, C.-C. 2007, J. Geophys. Res., 112, A06107

APPENDIX A: LIST OF SOLAR PROTON EVENTS

We list here the solar proton events analyzed in this study. See Table A1 for details.

Table A1. Solar Proton Events Affecting the Earth Environment (1996-2011)(collected from Space Weather Prediction Center of NOAA)

Solar Proton Event			Associated CME	Flare and Active Region				Solar Wind Speed		
Start (Day/UT)	Maximum (Day/UT)	Proton Flux (pfu @ > 10 MeV)	Onset (Direction/Day/UT)	Flare Maximum (Day/UT)	Importance (X Ray/Opt.)	Location	Region No.	SOHO	ACE	Mean
								($km\ s^{-1}$)		
1997.11.04/08:30	1997.11.04/11:20	72	W/04/06:10	1997.11.04/05:58	X2/2B	S14W33	8100	343		
1997.11.06/13:05	1997.11.07/02:55	490	W/06/>13:00	1997.11.06/11:55	X9/2B	S18W63	8100	425		
1998.04.20/14:00	1998.04.21/12:05	1700	W/20/10:07	1998.04.20/10:21	M1/EPL	S43W90	8194	377	354	366
1998.05.02/14:20	1998.05.02/16:50	150	Halo/02/14:06	1998.05.02/13:42	X1/3B	S15W15	8210	569	557	563
1998.05.06/08:45	1998.05.06/09:45	210	W/06/08:29	1998.05.06/08:09	X2/1N	S11W65	8210	437	461	449
1998.08.24/23:55	1998.08.26/10:55	670	NA	1998.08.24/22:12	X1/3B	N30E07	8307		651	
1998.09.25/00:10	1998.09.25/01:30	44	NA	1998.09.23/07:13	M7/3B	N18E09	8340		713	
1998.09.30/15:20	1998.10.01/00:25	1200	NA	1998.09.30/13:50	M2/2N	N23W81	8340		456	
1998.11.14/08:10	1998.11.14/12:40	310	NA	1998.11.14/05:18	C1/BSL	N28W90	8375?		407	
1999.01.23/11:05	1999.01.23/11:35	14	NA	1999.01.20/20:04	M5	N27E90			588	
1999.05.05/18:20	1999.05.05/19:55	14	Halo/03/06:06	1999.05.03/06:02	M4/2N	N15E32	8525	448	423	436
1999.06.04/09:25	1999.06.04/10:55	64	NW/04/07:26	1999.06.04/07:03	M3/2B	N17W69	8552	416	408	412
2000.02.18/11:30	2000.02.18/12:15	13	W/18/09:54	2000.02.17/20:35	M1/2N	S29E07	8872	368		
2000.04.04/20:55	2000.04.05/09:30	55	W/04/16:32	2000.04.04/15:41	C9/2F	N16W66	8933	394	382	388
2000.06.07/13:35	2000.06.08/09:40	84	Halo/06/15:54	2000.06.06/15:25	X2/3B	N20E18	9026	689	704	697
2000.06.10/18:05	2000.06.10/20:45	46	Halo/10/17:08	2000.06.10/17:02	M5/3B	N22W38	9026	479	468	474
2000.07.14/10:45	2000.07.15/12:30	24000	Halo/14/10:54	2000.07.14/10:24	X5/3B	N22W07	9077	398		
2000.07.22/13:20	2000.07.22/14:05	17	NW/22/12:30	2000.07.22/11:34	M3/2N	N14W56	9085	412	411	412
2000.09.12/15:55	2000.09.13/03:40	320	Halo/12/13:31	2000.09.12/12:13	M1/2N	S17W09	Filament	397	416	407
2000.10.16/11:25	2000.10.16/18:40	15	Halo/16/07:27	2000.10.16/07:28	M2	N04W90	9182?	527	544	536
2000.10.26/00:40	2000.10.26/03:40	15	Halo/25/08:26	2000.10.25/11:25	C4	N00W90		395	390	393
2000.11.24/15:20	2000.11.26/20:30	940	Halo/24/05:30	2000.11.24/05:02	X2/3B	N20W05	9236	530	585	558
2001.01.28/20:25	2001.01.29/06:55	49	Halo/28/15:54	2001.01.28/16:00	M1/1N	S04W59	9313	392	395	394
2001.03.29/16:35	2001.03.30/06:10	35	Halo/29/10:26	2001.03.29/10:15	X1/1N	N14W12	9393		450	
2001.04.02/23:40	2001.04.03/07:45	1110	NW/02/ 22:00	2001.04.02/21:51	X20	N18W82	9393	443	480	462
2001.04.10/08:50	2001.04.11/20:55	355	Halo/10/05:30	2001.04.10/05:26	X2/3B	S23W09	9415		724	
2001.04.15/14:10	2001.04.15/19:20	951	W/15/14:30	2001.04.15/13:50	X14/2B	S20W85	9415	409	496	453
2001.04.28/04:30	2001.04.28/05:00	57	Halo/26/12:30	2001.04.26/13:12	M7/2B	N17W31	9433	644	619	632
2001.09.15/14:35	2001.09.15/14:55	11	SW/15/11:54	2001.09.15/11:28	M1/1N	S21W49	9608	518	586	552
2001.09.24/12:15	2001.09.25/22:35	12900	Halo/24/10:30	2001.09.24/10:38	X2/2B	S16E23	9632	418		
2001.10.01/11:45	2001.10.02/08:10	2360	SW/01/05:30	2001.10.01/05:15	M9	S22W91	9628	445	483	464
2001.10.19/22:25	2001.10.19/22:35	11	Halo/19/16:50	2001.10.19/16:30	X1/2B	N15W29	9661	352	344	348
2001.10.22/19:10	2001.10.22/21:30	24	SE/22/18:26	2001.10.22/17:59	X1/2B	S18E16	9672	532	528	530
2001.11.04/17:05	2001.11.06/02:15	31700	Halo/04/16:35	2001.11.04/16:20	X1/3B	N06W18	9684	399	413	406
2001.11.19/12:30	2001.11.20/00:10	34	Halo/17/05:30	2001.11.17/05:25	M2/1N	S13E42	9704	522	509	516
2001.11.22/23:20	2001.11.24/05:55	18900	Halo/22/23:30	2001.11.22/23:30	M9/2N	S15W34	9704	428	467	448
2001.12.26/06:05	2001.12.26/11:15	779	W/26/05:30	2001.12.26/05:40	M7/1B	N08W54	9742	392	383	388
2001.12.29/05:10	2001.12.29/08:15	76	E/28/20:06	2001.12.28/20:45	X3	S26E90	9767	433	439	436
2002.02.20/07:30	2002.02.20/07:55	13	W/20/06:30	2002.02.20/06:12	M5/1N	N12W72	9825		400	
2002.03.17/08:20	2002.03.17/08:50	13	Halo/15/23:06	2002.03.15/23:10	M2/1F	S08W03	9866		278	

Solar Proton Event			Associated CME	Flare and Active Region				Solar Wind Speed		
Start (Day/UT)	Maximum (Day/UT)	Proton Flux (pfu @ > 10 MeV)	Onset (Direction/Day/UT)	Flare Maximum (Day/UT)	Importance (X Ray/Opt.)	Location	Region No.	SOHO	ACE	Mean ($km\ s^{-1}$)
2002.03.20/15:10	2002.03.20/15:25	19	W/18/02:54	2002.03.18/02:31	M1	S09W46	9866		555	
2002.04.17/15:30	2002.04.17/15:40	24	Halo/17/08:26	2002.04.17/08:24	M2/2N	S14W34	9906		520	
2002.04.21/02:25	2002.04.21/23:20	2520	W/21/01:27	2002.04.21/01:51	X1/1F	S14W84	9906		454	
2002.05.22/17:55	2002.05.23/10:55	820	Halo/22/03:26	2002.05.22/03:54	C5/DSF	S19W56			613	
2002.07.16/17:50	2002.07.17/16:00	234	Halo/15/20:30	2002.07.15/20:08	X3/3B	N19W01	30		476	
2002.08.14/09:00	2002.08.14/16:20	26	NW/14/02:06	2002.08.14/02:12	M2/1N	N09W54	61		489	
2002.08.22/04:40	2002.08.22/09:40	36	SW/22/02:00	2002.08.22/01:57	M5/2B	S07W62	69		439	
2002.08.24/01:40	2002.08.24/08:35	317	W/24/01:27	2002.08.24/01:12	X3/1F	S08W90	69		375	
2002.09.07/04:40	2002.09.07/16:50	208	Halo/05/16:54	2002.09.05/17:06	C5/DSF	N09E28	102		500	
2002.11.09/19:20	2002.11.10/05:40	404	SW/09/13:31	2002.11.09/13:23	M4/2B	S12W29	180		376	
2003.05.28/23:35	2003.05.29/15:30	121	Halo/28/00:50	2003.05.28/00:27	X3/2B	S07W17	365		653	
2003.05.31/04:40	2003.05.31/06:45	27	W/31/02:30	2003.05.31/02:24	M9/2B	S07W65	365		752	
2003.06.18/20:50	2003.06.19/04:50	24	Halo/17/23:30	2003.06.17/22:55	M6	S08E61	386		585	
2003.10.26/18:25	2003.10.26/22:35	466	Halo/26/17:54	2003.10.26/18:19	X1/1N	N02W38	484		482	
2003.10.28/12:15	2003.10.29/06:15	29500	Halo/28/10:54	2003.10.28/11:10	X17/4B	S16E08	486		790	
2003.11.04/22:25	2003.11.05/06:00	353	Halo/04/1954	2003.11.04/19:29	X28/3B	S19W83	486		580	
2003.11.21/23:55	2003.11.22/02:30	13	SW/21/00:26	2003.11.20/23:53	M5/2B	N02W17	501		494	
2004.04.11/11:35	2004.04.11/18:45	35	SW/11/04:30	2004.04.11/04:19	C9/1F	S14W47	588		440	
2004.07.25/18:55	2004.07.26/22:50	2086	Halo/25/15:30	2004.07.25/15:14	M1/1F	N08W33	652		783	
2004.09.13/21:05	2004.09.14/00:05	273	Halo/12/00:36	2004.09.12/00:56	M4/2N	N04E42	672		554	
2004.09.19/19:25	2004.09.20/01:00	57	W/19/22:24	2004.09.19/17:12	M1	N03W58	672		387	
2004.11.07/19:10	2004.11.08/01:15	495	Halo/07/17:06	2004.11.07/16:06	X2	N09W17	696		642	
2005.01.16/02:10	2005.01.17/17:50	5040	Halo/15/23:06	2005.01.15/23:02	X2	N15W05	720		586	
2005.05.14/05:25	2005.05.15/02:40	3140	Halo/13/17:22	2005.05.13/16:57	M8/2B	N12E11	759		556	
2005.06.16/22:00	2005.06.17/05:00	44	W/16/20:03	2005.06.16/20:22	M4	N09W87	775		592	
2005.07.14/02:45	2005.07.15/03:45	134	Halo/13/14:30	2005.07.13/14:49	M5	N10W80	786		430	
2005.07.27/23:00	2005.07.29/17:15	41	Halo/27/04:54	2005.07.27/05:02	M3	N11E90	792		554	
2005.08.22/20:40	2005.08.23/10:45	330	Halo/22/17:30	2005.08.22/17:27	M5/1N	S12W60	798		457	
2005.09.08/02:15	2005.09.11/04:25	1880	E/07/17:23	2005.09.07/17:40	X17/3B	S06E89	808		873	
2006.12.06/15:55	2006.12.07/19:30	1980	Halo	2006.12.05/10:35	X9/2N	S07E79	930		580	
2006.12.13/03:10	2006.12.13/09:25	698	Halo/13/02:54	2006.12.13/02:40	X3/4B	S05W23	930		641	
2010.08.14/12:30	2010.08.14/12:45	14	W/14/13:25	2010.08.14/10:05	C4/0F	N17W52	1099		409	
2011.03.08/01:05	2011.03.08/08:00	50	NW/07/20:00	2011.03.07/20:12	M3/SF	N24W59	1164		379	
2011.06.07/08:20	2011.06.07/18:20	72	SW/08/17:50	2011.06.07/08:03	M2/2N	S21W64	1226		457	
2011.08.04/06:35	2011.08.05/21:50	96	NW/06/05:15	2011.08.04/04:12	M9/2B	N15W49	1261		583	
2011.08.09/08:45	2011.08.09/12:10	26	NW/09/17:10	2011.08.09/08:05	X6/2B	N17W83	1263		588	
2011.09.23/22:55	2011.09.26/11:55	35	NE/27/04:30	2011.09.22/11:01	X1/2N	N11E74	1302		428	
2011.11.26/11:25	2011.11.27/01:25	80	NW/28/01:45	2011.11.26/07:10	C1	N08W49	1353		358	

This paper has been typeset from a TEX/LATEX file prepared by the author.